nature geoscience

LETTERS

PUBLISHED ONLINE: 22 NOVEMBER 2009 | DOI: 10.1038/NGEO697

Migration of early aftershocks following the 2004 Parkfield earthquake

Zhigang Peng* and Peng Zhao

Large shallow earthquakes are immediately followed by numerous aftershocks. A significant portion of these events is missing in existing earthquake catalogues, mainly because seismicity after the mainshock can be masked by overlapping arrivals of waves from the mainshock and aftershocks[1–4]. However, recovery of the missing early aftershocks is important for understanding the physical mechanisms of earthquake triggering[2–4], and for tracking postseismic deformation around the rupture zone associated with the mainshock[5–7]. Here we use the waveforms of 3,647 relocated earthquakes[8] along the Parkfield section of the San Andreas fault as templates[9,10] to detect missing aftershocks within three days of the 2004 magnitude 6.0 Parkfield earthquake. We identify 11 times more aftershocks than listed in the standard catalogue of the Northern California Seismic Network. We find that the newly detected aftershocks migrate in both along-strike and down-dip directions with logarithmic time since the mainshock, consistent with numerical simulations of the expansion of aftershocks caused by propagating afterslip[11,12]. The cumulative number of early aftershocks increases linearly with postseismic deformation in the first two days, supporting the view that aftershocks are driven primarily by afterslip[13,14].

The Parkfield section of the San Andreas fault (SAF) straddles the transition between the creeping segment to the northwest and the locked segment to the southeast (Fig. 1). The 28 September 2004 M_w 6.0 Parkfield earthquake nucleated near Gold Hill south of Parkfield, and the rupture propagated predominately in the northwest direction towards Middle Mountain with a total length of ~30 km (ref. 15). The mainshock and its numerous aftershocks were recorded continuously by many near-field seismic instruments, resulting in one of the best recorded earthquake sequences in the world.

We use waveforms of 3,647 earthquakes listed in the relocated catalogue[8] as templates to detect missing events within three days since 28 September 2004 (see the Methods section). Figure 2 shows an example of a positive detection on 28 September 2004 at 17:17:44, approximately 140 s after the origin time of the mainshock (28 September 2004 17:15:24). Although two more events occurred within 10 s, the matched filter technique is able to uniquely identify the target event with a network-averaged cross-correlation coefficient of 0.79. It is worth noting that none of these newly detected events (in the magnitude range of 2.4–2.6) is listed in the Northern California Seismic Network (NCSN) catalogue. Overall, we have a total of 610,286 positive detections between 28 and 30 September 2004. After removing multiple detections (see the Methods section), we obtain 11,138 individual events. In comparison, only 543 and 933 events were listed in the Thurber *et al.*[8] and the NCSN catalogues, respectively. Hence, our matched filter technique has detected at least 11 times more aftershocks than those in the NCSN catalogue. A detailed comparison of the locations, magnitudes and statistical properties between our detected events and the NCSN catalogue is given in Supplementary Notes S1,S2.

Figure 3a shows the locations of the detected aftershocks colour-coded by their occurrence times since the mainshock in a logarithmic timescale. Detailed views of all aftershocks in the first hour and within two days after the mainshock are shown in Supplementary Movies. We find that aftershocks within the first hour mainly occurred along a 12-km-long 'streak' at the depth range of 4–6 km (ref. 8), just above a large patch of high slip 10–20 km north of the epicentre at the depth range of 5–7 km (refs 15–18). In comparison, aftershocks in another seismic 'streak' at the depth range of 8–10 km were not as active as those in the shallow 'streak' (Supplementary Fig. S6). Finally, a cluster of deep events at 13 km beneath Middle Mountain and the region north of the San Andreas Fault Observatory at Depth (SAFOD) in the creeping section were not active within the first few hours after the mainshock (Supplementary Figs S6,S7), indicating a possible migration of aftershocks along the SAF strike and the down-dip directions.

To investigate this further, Fig. 3b shows the occurrence time since the mainshock against the along-strike distance for all events within 2 km of the SAF. The newly detected events show clear migration with logarithmic time in the creeping section of the SAF. The migration speed is ~3.4 km decade^{-1} since the mainshock. In comparison, the aftershocks southeast of our study region seem to expand suddenly from 7 to 17 km southeast of the epicentre around 10^4 s (~3 h) after the mainshock, rather than migrating with time as shown in the creeping section. We also examine the NCSN catalogue, which covers a wider region than the Thurber *et al.*[8] catalogue, and find a similar but weaker migration pattern (Supplementary Fig. S8).

Next, we separate all aftershocks into three depth ranges and compare their along-strike migration patterns (Supplementary Fig. S9). A general feature is that aftershocks show clear expansion in the creeping section at three depth ranges. Furthermore, the expansion speed in the top 3 km is faster than those at larger depths. We also examine the temporal evolutions of the hypocentral depths for the detected aftershocks by separating all of the aftershocks according to the seismicity distributions (Supplementary Fig. S10). We find that the aftershocks at shallow depth in the creeping section northwest of Middle Mountain and beneath Middle Mountain seem to migrate in the up-dip direction. In comparison, the down-dip migration at larger depth is best shown in segments beneath and southwest of Middle Mountain.

One potential cause of the apparent migration shown in Fig. 3 and Supplementary Figs S9,S10 is an increase in the number of samples by plotting the time axis in a logarithmic scale. We have examined this in detail and found that although such bias does exist in our data, the observed patterns cannot be caused by plotting alone or random occurrence, but rather represent a

School of Earth and Atmospheric Sciences, Georgia Institute of Technology, Atlanta, Georgia 30332, USA. *e-mail: zpeng@gatech.edu.

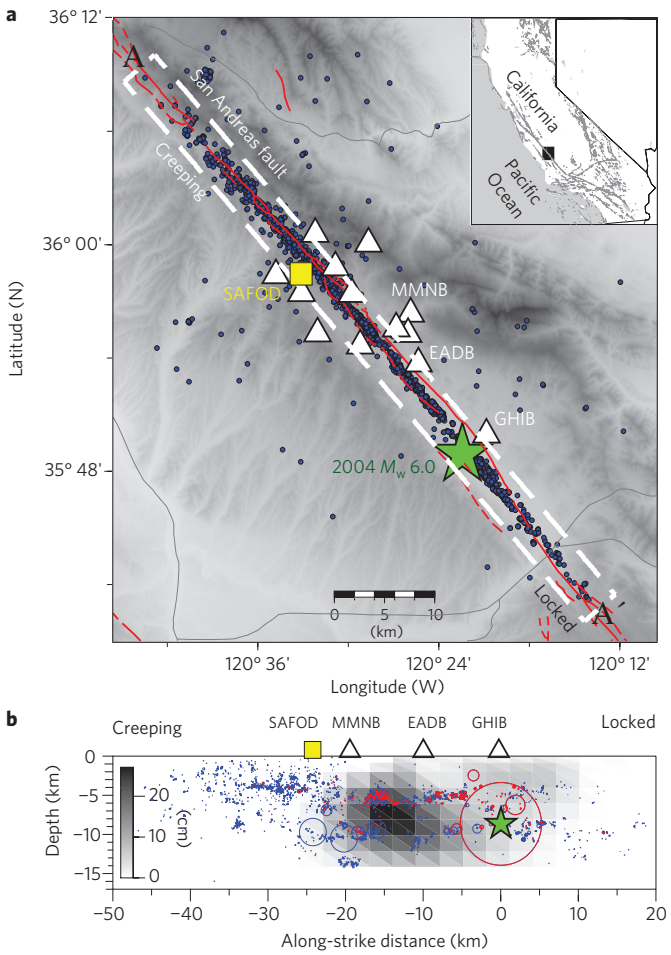

Figure 1 | Map of the SAF and the 2004 Parkfield earthquake sequence. **a**, Map of the Parkfield section of the SAF (red line), including the epicentral location of the 2004 M_w 6.0 Parkfield earthquake (green star), and the 3,647 template events listed in the relocated catalogue[8] (blue dots). The open triangles represent 13 stations in the HRSN, with selected station names marked. The San Andreas Fault Observatory at Depth (SAFOD) is denoted by the yellow square. **b**, The cross-section view of the 3,647 template events (blue) along the SAF, and those detected within the first hour after the Parkfield mainshock (red). The size is computed by assuming a circular crack model and a constant stress drop of 3 MPa. The background shading denotes the mainshock slip distribution[17].

unique combination of space-time migration immediately after the mainshock (see Supplementary Note S6). We also find that other migration functions do not provide a better fit to the propagating seismicity front than the $\log(t)$ functions.

It has been long recognized that aftershocks often migrate along the fault strike and down-dip directions[5,6,19]. In some cases, aftershock zones show little expansion[5], whereas in other cases, aftershock zones grow rapidly during the first few days following the mainshock, and the expansion slows down at a later time[5,6,19]. Such spatio-temporal migrations offer important clues on the physical mechanisms of aftershock generation. The temporal decay and spatial expansion of aftershocks could be explained by a delayed response to the coseismic stress changes for populations of faults around the mainshock rupture obeying the laboratory-derived rate–state friction law[20]. Alternatively, recent observations of aftershocks and postseismic deformation following an Omori-law-type decay with similar relaxation times have led to the suggestion that aftershocks are driven primarily by aseismic afterslip around the mainshock rupture zone[13,14]. Other possible mechanisms to trigger aftershocks include dynamic stress changes from passing seismic waves[21], viscoelastic relaxation in the lower crust and upper mantle, or by fluid flows[22].

Many previous studies have found that postseismic deformation following the 2004 Parkfield earthquake mostly occurs as afterslip within the aseismic creeping patches of the SAF surrounding the locked asperity[16,18,23,24]. The cumulative moment release from afterslip in two years after the mainshock is about three times the coseismic moment release[18], suggesting that quasi-static stress changes from afterslip may have a more important role in triggering aftershocks than static stress changes from the Parkfield mainshock. Furthermore, the cumulative number of the Parkfield aftershocks and the postseismic deformation seem to be linearly related[18,25,26], and the cumulative seismic moment of aftershocks is only ~1% of the geodetic moment owing to afterslip[18]. These observations imply that both the postseismic relaxation and aftershocks following the 2004 Parkfield mainshock were primarily driven by afterslip. Here we also find that the cumulative number of the newly detected aftershocks with magnitude $M > 1.5$ increases linearly with postseimic deformation in the first two days (see Supplementary Note S7). However, the early aftershocks are too many to match the linear relationship established a few days after the mainshock, consistent with previous findings[26].

Although the temporal behaviour of cumulative aftershocks seems to be related to postseismic relaxation, their spatial evolutions have not been analysed in detail previously. Recently, Kato[12] conducted three-dimensional numerical simulations to investigate the relationships among aftershocks, afterslip, effective normal stress σ_{eff} (that is, the normal stress minus the pore pressure) and frictional parameters a and b of the laboratory-derived rate–state-dependent friction law[20]. The simulation shows that the radius of the aftershock area expands logarithmically with time since the mainshock, consistent with our observations. Furthermore, the rate of aftershock expansion is inversely proportional to the value of A–B ($=(a-b)\sigma_{\mathrm{eff}}$; ref. 12). These results further support the casual link between afterslip and aftershocks, and allow us to draw inference regarding the frictional parameters of the SAF from aftershock migration. As shown in Fig. 3, the aftershock area increases from ~32 km at 100 s to ~48 km at 10^5 s after the mainshock. Such expansion is roughly compatible with the migration of simulated aftershocks[12] in the velocity-strengthening region with the value of A–B in the range of 0.2–0.5 MPa (Supplementary Note S8). Assuming an effective normal stress of 50 MPa (ref. 16), the corresponding value of a–b is in the range of 0.004–0.01, which is close to the value of 0.007 obtained by geodetic inversion of Barbot *et al.*[18], and higher than the value of 0.0001–0.002 obtained by Johnson and colleagues[16]. We note that the frictional parameters a and b are probably not fixed values, but could vary significantly along the fault strike and depth. Furthermore, the effective normal stress σ_{eff} probably increases with depth. Such a depth-dependent effect could explain the difference in the migration speed for the shallow and deep aftershocks[11].

If the aftershocks following the 2004 Parkfield mainshock were primarily driven by afterslip[18,25,26], an expansion of aftershocks would suggest an outward propagating afterslip from the mainshock rupture area. Recent studies based on kinematic and rate–state slip inversions have shown that afterslip of the 2004 Parkfield earthquake mainly occurs around the mainshock rupture zone in the top 5 km immediately after the mainshock, and spreads laterally and with depth afterwards[16,18]. This pattern is largely compatible with our observations of aftershock migration in the along-strike and down-dip directions. We also observed that the shallow seismicity (that is, depth < 2 km) in the creeping section and beneath Middle Mountain did not occur until a few hours after the mainshock (Supplementary Figs S9,S10). This is consistent with both field[27] and geodetic[23] observations of delayed surface slip a

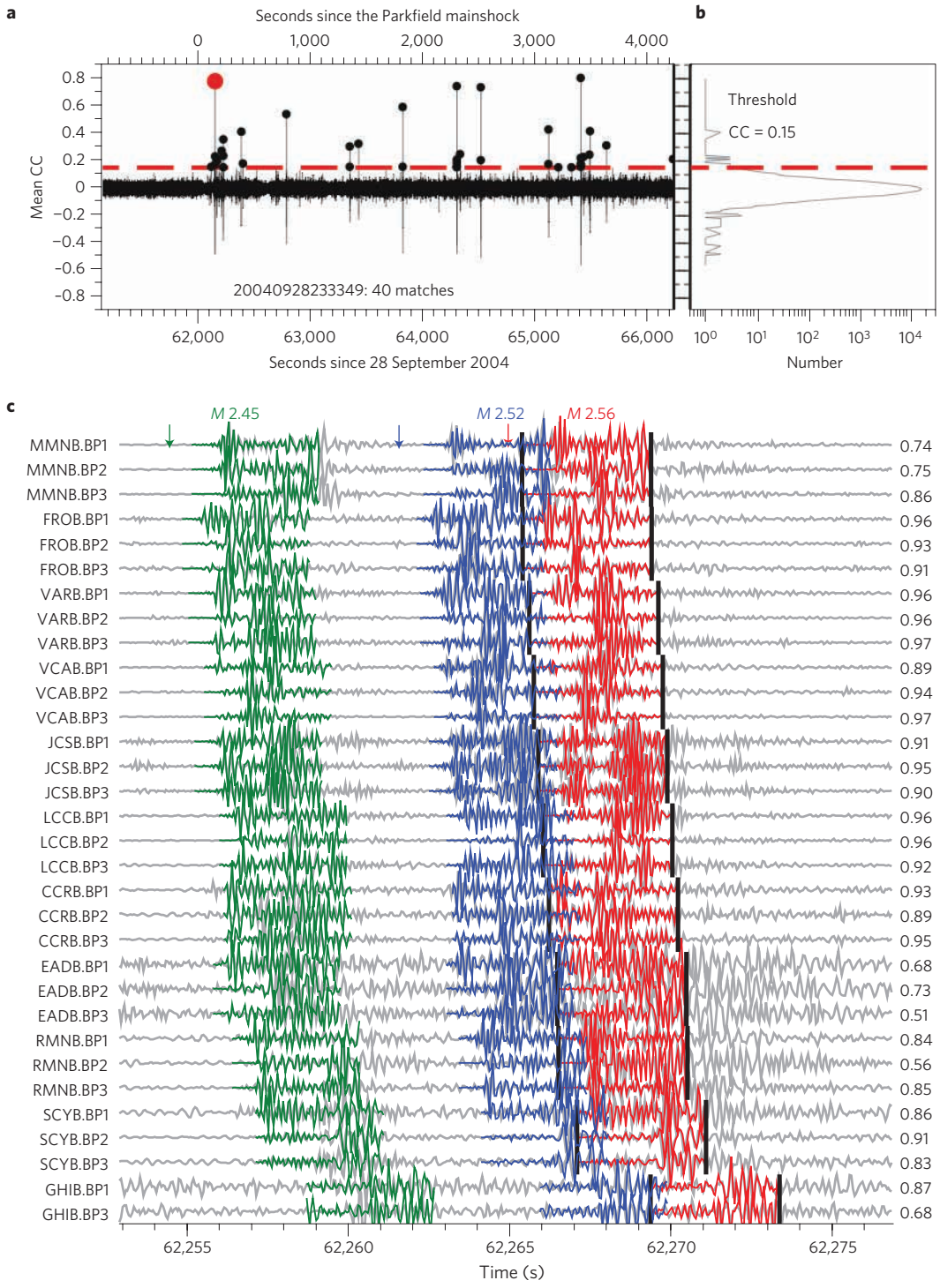

Figure 2 | Example of a detected early aftershock. a, Mean cross-correlation (CC) functions for the template event 20040928233349. The black dots are positive detections above the threshold (red dashed line) and the red dot corresponds to the detected *M* 2.56 event at ~140 s after the mainshock. **b**, The histogram of the mean correlation coefficient functions. **c**, A comparison of the template waveforms (red) and the continuous waveforms (grey) for each component of 11 stations. The waveforms shown in green and blue correspond to two other events that occurred nearby. The arrows mark the origin times of the three events. The station and channel names and the corresponding cross-correlation values are labelled on the left and right sides, respectively.

few hours following the mainshock, suggesting a propagation of afterslip in the up-dip direction. A recent study has shown that non-volcanic tremor near Monarch Peak (~50–60 km northwest of the Parkfield epicentre) became activated ~10 days after the mainshock[28]. Such a delayed response could also be related to the slow propagation of afterslip in the creeping section as inferred from this and other studies[16,18]. However, another study based on the principal component analysis suggested that the locus of afterslip has not changed much over time in the first 900 days after the mainshock[26]. At least part of the discrepancy arose from the inclusion of the first few minutes of postseismic measurement in the study of Johnson *et al.*[16], and uncertainties of slip inversion at larger depth. Further studies are needed to clarify whether early afterslip following the Parkfield mainshock

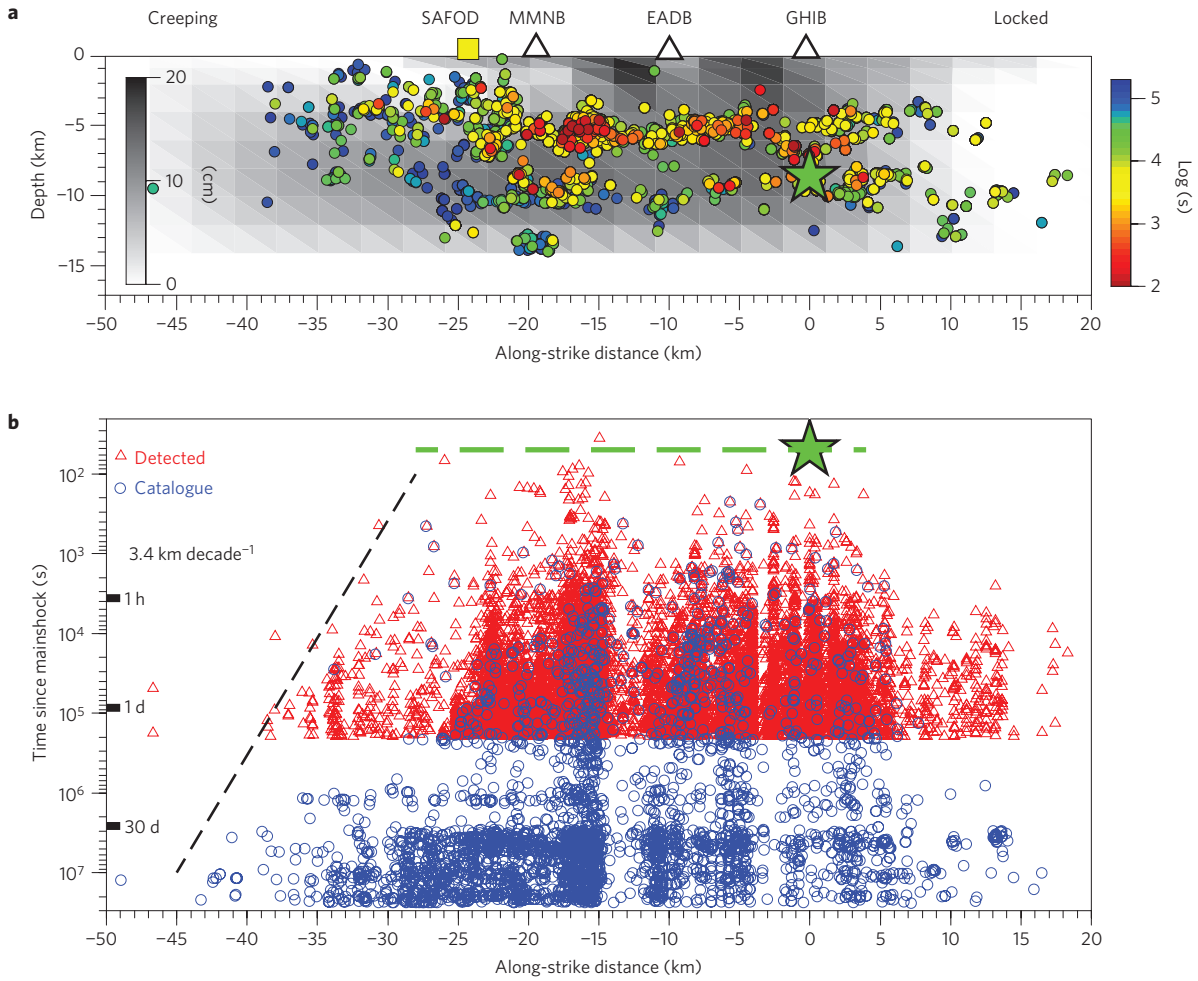

Figure 3 | Migration of the Parkfield early aftershocks. a, The cross-section view of all the detected events along the SAF colour-coded by the logarithmic time after the mainshock (green star). The background shading denotes the cumulative afterslip in the first 60 days[17]. **b**, The occurrence times of aftershocks since the 2004 Parkfield mainshock versus the along-strike distances. The blue circles and the red triangles mark the events listed in the Thurber *et al.*[8] catalogue and detected by the matched filter technique, respectively. The black dashed line marks the approximate slope of aftershock migration along the creeping section of the SAF.

propagates outward with time, similar to what has been observed for early aftershocks.

As mentioned before, many physical models have been proposed to explain aftershock triggering. These include coseismic stress changes[20], afterslip[13,14] or a combined effect of coseismic stress changes and afterslip following the mainshock[14,20,29]. The seismicity rates predicted by these different models all follow Omori's law-type decay at later times, but differ from each other immediately after the mainshock[20,29]. We did not attempt to distinguish among these different models from the temporal decay rate of aftershocks in this study, mainly because our catalogue is still not complete in the first 100 s after the Parkfield mainshock, owing to clipping of the High Resolution Seismic Network (HRSN) recordings in the first 30–50 s, and the long-lasting mainshock coda in the 2–8 Hz frequency range (Supplementary Note S9). Instead, we focused on the spatio-temporal evolutions of early aftershocks in an unprecedented detail, based on the 11-fold increase of aftershock detections from the matched filter technique[9,10]. The early aftershocks showed clear migration in along-strike and down-dip directions with the logarithmic time since the mainshock. So the aftershock expansion is most significant immediately after the mainshock, consistent with previous observations[5–7,19] and recent numerical simulations[12]. Our results suggest that systematic detection and analysis of early aftershocks not only provide important constraints on the mainshock rupture properties and aftershock migration patterns, but also shed new insights into postseismic deformation and frictional properties of the active fault zones.

Methods

The analysis procedure generally follows that of Shelly *et al.*[10] and is briefly described here. The seismic data are recorded by the 13 three-component short-period borehole stations of the HRSN operated by University of California, Berkeley. We use three-component seismograms with 20 samples s^{-1} as templates, and search through three-day continuous recordings since 28 September 2004 to detect seismic events by waveform cross-correlation. A two-way fourth-order 2–8 Hz Butterworth filter is applied to both the template and continuous waveforms. Next, we compute the P- and S-wave arrival times for each event using a one-dimensional velocity model in this region[30] with a nominal V_P/V_S ratio of 1.732. A 4 s time window starting 2 s before the computed S-wave arrivals is used as the waveform template window (signal). The noise level is obtained from a 4 s time window 6 s before the computed P-wave arrivals. We require that each template event be recorded by at least 4 out of the 13 stations (12 channels) with a minimum signal-to-noise ratio of 5. Futhermore, each template event needs to have a magnitude that can be used to calibrate the magnitude of the detected event. After the section process, we obtain a total of 3,647 earthquakes listed in the relocated catalogue[8] as our template events.

We shift the 4 s time window around the computed S-wave arrival in an increment of 0.05 s (1 sample) through the three-day continuous waveforms. At each time point, we compute the correlation coefficient, and assign the correlation coefficient value to its origin time by subtracting the computed S-wave arrival time. Next, we stack the correlation coefficient values for all stations and three components, and compute the mean correlation coefficient value at each time

point, which is used as a measure of similarity between the template and detected events. We compute the median absolute deviation (MAD) of the mean correlation coefficient trace for each template event and use nine times the MAD as the detection threshold[10]. For a normally distributed random variable, the standard deviation s is 1.4826 × MAD. The corresponding probability of exceedance for 9 times the MAD, or 5.4 times the standard deviation σ, is 6.4×10^{-10}. In a one-day period, we sample 172,800 time steps for each template event. So the chance of random detection using the threshold of 9 × MAD is about one event per day, suggesting that most of the detections correspond to real events, instead of false detection by random chance.

As the detected events have similar waveforms at multiple stations as compared to the template event, their hypocentre locations must be close or identical[10]. We assign the location of the detected event to that of the template event. For multiple detections in each 2 s window, we assign the location of the template event with the highest mean correlation coefficient value[10]. The origin time of the detected event is simply the time associated with the highest mean correlation coefficient value. Finally, we compute the magnitude of the detected event based on the median value of the maximum amplitude ratios for all channels between the template and detected events, assuming that a tenfold increase in amplitude corresponds to one unit increase in magnitude.

Received 12 August 2009; accepted 22 October 2009; published online 22 November 2009

References

1. Kagan, Y. Y. Short-term properties of earthquake catalogues and models of earthquake source. *Bull. Seismol. Soc. Am.* **94,** 1207–1228 (2004).
2. Peng, Z., Vidale, J. E. & Houston, H. Anomalous early aftershock decay rates of the 2004 M6 Parkfield earthquake. *Geophys. Res. Lett.* **33,** L17307 (2006).
3. Peng, Z., Vidale, J. E., Ishii, M. & Helmstetter, A. Seismicity rate immediately before and after main shock rupture from high-frequency waveforms in Japan. *J. Geophys. Res.* **112,** B03306 (2007).
4. Enescu, B., Mori, J. & Miyazawa, M. Quantifying early aftershock activity of the 2004 mid-Niigata Prefecture earthquake (M_w 6.6). *J. Geophys. Res.* **112,** B04310 (2007).
5. Tajima, F. & Kanamori, H. Global survey of aftershock area expansion patterns. *Phys. Earth Planet. Inter.* **40,** 77–134 (1985).
6. Henry, C. & Das, S. Aftershock zones of large shallow earthquakes: Fault dimensions, aftershock area expansion and scaling relations. *Geophys. J. Int.* **147,** 272–293 (2001).
7. Chang, C.-H., Wu, Y.-M., Zhao, L. & Wu, F.-T. Aftershocks of the 1999 Chi–Chi, Taiwan, Earthquake: The first hour. *Bull. Seismol. Soc. Am.* **97,** 1245–1258 (2007).
8. Thurber, C. *et al.* Three-dimensional compressional wavespeed model, earthquake relocations, and focal mechanisms for the Parkfield, California, region. *Bull. Seismol. Soc. Am.* **96,** S38–S49 (2006).
9. Gibbons, S. J. & Ringdal, F. The detection of low magnitude seismic events using array-based waveform correlation. *Geophys. J. Int.* **165,** 149–166 (2006).
10. Shelly, D. R., Beroza, G. C. & Ide, S. Non-volcanic tremor and low-frequency earthquake swarms. *Nature* **446,** 305–307 (2007).
11. Ariyoshi, K., Matsuzawa, T. & Hasegawa, A. The key frictional parameters controlling spatial variations in the speed of postseismic-slip propagation on a subduction plate boundary. *Earth Planet. Sci. Lett.* **256,** 136–146 (2007).
12. Kato, N. Expansion of aftershock areas caused by propagating post-seismic sliding. *Geophys. J. Int.* **168,** 797–808 (2007).
13. Perfettini, H. & Avouac, J.-P. Postseismic relaxation driven by brittle creep: A possible mechanism to reconcile geodetic measurements and the decay rate of aftershocks, application to the Chi–Chi earthquake, Taiwan. *J. Geophys. Res.* **109,** B02304 (2004).
14. Hsu, Y. J. *et al.* Frictional afterslip following the 2005 Nias-Simeulue earthquake, Sumatra. *Science* **312,** 1921–1926 (2006).
15. Bakun, W. H. *et al.* Implications for prediction and hazard assessment from the 2004 Parkfield earthquake. *Nature* **437,** 969–974 (2005).
16. Johnson, K. M., Burgmann, R. & Larson, K. Frictional properties on the San Andreas Fault near Parkfield, California inferred from models of afterslip following the 2004 earthquake. *Bull. Seismol. Soc. Am.* **96,** S321–S338 (2006).
17. Murray, J. & Langbein, J. Slip on the San Andreas Fault at Parkfield, California, over two earthquake cycles, and the implications for seismic hazard. *Bull. Seismol. Soc. Am.* **96,** S283–S303 (2006).
18. Barbot, S., Fialko, Y. & Bock, Y. Postseismic deformation due to the M_w 6.0 2004 Parkfield earthquake: Stress-driven creep on a fault with spatially variable rate-and-state friction parameters. *J. Geophys. Res.* **114,** B07405 (2009).
19. Chatelain, J.-L., Cardwell, R. K. & Isacks, B. L. Expansion of the aftershock zone following the Vanuatu (New Hebrides) earthquake on 15 July 1981. *Geophys. Res. Lett.* **10,** 385–388 (1983).
20. Dieterich, J. A constitutive law for rate of earthquake production and its application to earthquake clustering. *J. Geophys. Res.* **99,** 2601–2618 (1994).
21. Hill, D. P. & Prejean, S. G. in *Earthquake Seismology Treatise on Geophysics* (ed. Kanamori, H.) (Elsevier, 2007).
22. Nur, A. & Booker, J. R. Aftershocks caused by pore fluid flow? *Science* **175,** 885–888 (1972).
23. Langbein, J., Murray, J. & Snyder, H. A. Coseismic and initial postseismic deformation from the 2004 Parkfield, California, earthquake, observed by Global Positioning System, creepmeters, and borehole strainmeters. *Bull. Seismol. Soc. Am.* **96,** S304–S320 (2006).
24. Freed, A. M. Afterslip (and only afterslip) following the 2004 Parkfield, California, earthquake. *Geophys. Res. Lett.* **34,** L06312 (2007).
25. Savage, J. C. & Yu, S.-B. Postearthquake relaxation and aftershock accumulation linearly related after 2003 Chengkung (M6.5, Taiwan) and 2004 Parkfield (M6.0, California) earthquakes. *Bull. Seismol. Soc. Am.* **97,** 1632–1645 (2007).
26. Savage, J. C. & Langbein, J. Postearthquake relaxation after the 2004 M6 Parkfield, California, earthquake and rate-and-state friction. *J. Geophys. Res.* **113,** B10407 (2008).
27. Rymer, M. J. *et al.* Surface fault slip associated with the 2004 Parkfield, California, Earthquake. *Bull. Seismol. Soc. Am.* **96,** S11–S27 (2006).
28. Nadeau, R. M. & Guilhem, A. Nonvolcanic tremor evolution and the San Simeon and Parkfield, California earthquakes. *Science* **325,** 191–193 (2009).
29. Helmstetter, A. & Shaw, B. E. Afterslip and aftershocks in the rate-and-state friction law. *J. Geophys. Res.* **114,** B01308 (2009).
30. Waldhauser, F., Ellsworth, W. L., Schaff, D. P. & Cole, A. Streaks, multiplets, and holes: High-resolution spatio-temporal behavior of Parkfield seismicity. *Geophys. Res. Lett.* **31,** L18608 (2004).

Acknowledgements

The seismic data used in this study are recorded by the HRSN operated by Berkeley Seismological Laboratory, University of California, Berkeley, and are distributed by the Northern California Earthquake Data Center (NCEDC). We thank D. Shelly, K. Koper and C. Wu for their help in generating Supplementary Movies, N. Kato for sharing the results from the numerical simulation in the Kato[12] paper, S. Barbot, K. Johnson, P.-C. Liu and J. Murray-Moraleda for sharing their mainshock slip inversion and afterslip models, and J. Savage for sharing the data from the principal component analysis in the Savage and Langbein[26] paper. The manuscript benefited from useful comments by J.-P. Avouac, R. Bergmann, B. Enescu, H. Houston, K. Johnson, N. Kato, O. Lengline, J. Savage, D. Shelly and J. Vidale. This work is supported by the USGS NEHRP program G09AP00114.

Author contributions

Z.P. designed the project; Z.P. and P.Z. carried out the data analysis; Z.P. wrote the manuscript with contributions from P.Z.

Additional information

Supplementary information accompanies this paper on www.nature.com/naturegeoscience. Reprints and permissions information is available online at http://npg.nature.com/reprintsandpermissions. Correspondence and requests for materials should be addressed to Z.P.